Correlations and ground-state transitions of few-electron quantum dots in a strong magnetic field

1999 J. Phys.: Condens. Matter 11 435

(http://iopscience.iop.org/0953-8984/11/2/010)

J. Phys.: Condens. Matter **11** (1999) 435–454. Printed in the UK PII: S0953-8984(99)93365-9

Correlations and ground-state transitions of few-electron quantum dots in a strong magnetic field

W Y Ruan†‡§ and Ho-Fai Cheung‡

† Department of Applied Physics, South China University of Technology, Guangzhou 510641, People's Republic of China
‡ Department of Physics and Material Science, City University of Hong Kong, Kowloon, Hong Kong, People's Republic of China

Received 16 April 1998, in final form 9 November 1998

Abstract. We present numerical results for the low-lying spectra of quantum dots with $N = 3$ to 8 as a function of the external magnetic field. The only values that the angular momentum of the ground state can take are magic values. This is interpreted in terms of a geometrical configuration model and an ℓ-configuration model. The relationship of the two models is discussed.

1. Introduction

With the use of modern lithographic techniques and through a series of masking and etching steps, it is now possible to create a single quantum dot containing N ($N = 1, 2, 3, \ldots$) electrons [1–9]. The resulting dot has typically a disc-like shape with a lateral confinement potential that to a good approximation is parabolic. In such quantum dots the gate potential and thus the number of electrons can be controlled at will. Single-electron capacitance spectroscopy allows indirect measurement of the energy levels of a single dot [7, 9].

Theoretical considerations of systems of few electrons in two space dimensions and a perpendicular magnetic field can be traced back to the early 1980s. The three-electron system with parabolic *pressure* was first considered by Laughlin in the context of the fractional quantum Hall effect [10]; this essentially laid the groundwork for studies on quantum dots. Laughlin explicitly constructed the spin-polarized correlated states in the lowest Landau level and showed that they approximate the exact eigenstates well. The ground state turned out to be incompressible over a range of applied pressure because only *magic* values of the angular momentum $L = 3k$ ($k = 1, 2, 3, \ldots$) minimize the interaction energy. Similar analysis was later carried out by Girvin and Jach [11], and Lai *et al* up to $N = 7$ [12]; the magic numbers were found to exist for systems with more particles.

The role of electron–electron interactions, and the effects of confinement and external magnetic field on few-electron quantum dots have been studied by Maksym and Chakraborty for $N = 3, 4$ [13], and Yang *et al* for $N = 5, 6$ [14]. Using a direct numerical diagonalization technique, they calculated the energy spectra of the dots in the polarized and unpolarized states, and pointed out the competition of the kinetic and interaction energies. As a result of this competition, the angular momentum of the ground state of a few-electron system changes with increasing magnetic field through a series of magic numbers. This predicted transition has

§ E-mail address: phwyruan@scut.edu.cn.

0953-8984/99/020435+20$19.50

recently been confirmed in experiments for $N = 2, 3$ [15]. The existence of magic numbers is also predicted to cause oscillations in physical properties such as the electronic specific heat [13], magnetization [16], and magnetoluminescence [17], and to affect the transport [18], and the chemical potential [19].

As for the origin of the magic numbers, several theoretical explanations have been proposed. In the composite-fermion model [20, 21], Jain *et al* constructed a trial ground-state wavefunction in the following form:

$$\Psi_L(z_1, z_2, \ldots, z_N) = \hat{P}_a \prod_{i>j} (z_i - z_j)^{2k} \Phi_{L^*} \tag{1}$$

where $L = L^* + kN(N-1)$, and $\hat{P}_a$ projects the wavefunction onto the lowest Landau level (see below); L^* is subject to the condition $-N(N-1)/2 \leqslant L^* \leqslant N(N-1)/2$; Φ_{L^*} is the wavefunction of non-interacting electrons with total angular momentum L^*. They argued that all possible magic numbers must identify such states Φ_{L^*} where the electrons compactly fill each Landau level from the lowest possible angular momentum. The composite-fermion model captures most of the physics since the wavefunction given by equation (1) normally has an overlap close to unity with the true state. However, it turns out that the compact filling is neither a necessary condition, since it rejects some important magic numbers, nor a sufficient condition, since not all compact fillings give a particularly low interaction energy [22]. Thus with the composite-fermion model one does not know which L should be a magic number beforehand. Recently, on the basis of the concept of sub-Landau-level structures, a *pocket calculator* model was proposed by Dharma-wardana for predicting the magic numbers and the ground-state energy [23]. Unfortunately, Dharma-wardana's model was only partly successful [24].

The pair-correlation functions of groups of few electrons have been analysed in some detail by Maksym [25, 26]. Using the Eckart-frame approach, Maksym found that at large L the dot has molecule-like electronic structures when there is only one equilibrium configuration, and has liquid-like structures when there is more than one equilibrium configuration. In some recent studies [27, 28], we have argued that the origin of the magic numbers must be the symmetry constraints on the geometrical configuration (this is known as the geometrical configuration model; it deals with the magic numbers in the polarized and unpolarized states in a unified manner); we made a detailed calculation for the three-electron and four-electron dots in the Wigner-crystal regime, and found that the model predicted the magic numbers well.

The main objective of this paper is to further clarify the origin of the magic numbers. In the following section the quantum dot model and the numerical method are described. Extensive numerical results for the low-lying spectra for systems of few electrons are presented in section 3. In section 4, the basic idea of the geometrical model is recalled and the model is reformulated in a more general fashion. In addition to the geometrical model, a model in the space of single-particle angular momentum, called the ℓ-configuration model, is proposed which seems to work better than the geometrical model at small L. Its equivalence to the geometrical configuration model is revealed.

2. Formalism

Let us consider the motion of a single electron in a parabolic potential, $\frac{1}{2}m^*\omega_0^2 r^2$, in the X–Y plane with a uniform magnetic field $\boldsymbol{B}$ applied in the $-Z$-direction; the single-particle Hamiltonian is

$$h = h_{\text{space}} + h_{\text{spin}} \tag{2}$$

$$h_{\text{space}} = \frac{1}{2m^*}(\boldsymbol{p} + e\boldsymbol{A})^2 + \frac{1}{2}m^*\omega_0^2 r^2 \tag{3}$$

$$h_{\text{spin}} = -g^*\mu_B B\hat{s}_z \tag{4}$$

where m^* is the effective electron mass, ω_0 is a strength parameter for the confinement potential, g^* is the effective Landé factor, μ_B is the Bohr magneton, and $\hat{s}_z$ is the spin operator in the Z-direction. With a symmetric gauge, $\boldsymbol{A} = \boldsymbol{B} \times \boldsymbol{r}/2$, equation (3) can be rewritten as

$$h_{\text{space}} = \frac{p^2}{2m^*} + \frac{1}{2}m^*\omega^2 r^2 - \frac{\omega_c}{2}\hat{\ell} \tag{5}$$

where $\omega = \sqrt{\omega_0^2 + \omega_c^2/4}$, $\omega_c = eB/m^*$ is the cyclotron frequency, and $\hat{\ell}$ is the angular momentum operator in the Z-direction. The eigenstates of h_{space} are given by

$$|kl\rangle = N_{kl} z^l L_k^{|l|}[|z|^2/(2a^2)] \exp[-|z|^2/(4a^2)] \tag{6}$$

where

$$N_{kl} = \sqrt{k!/[2^{|l|+1}\pi(k + |l|)!a^{2(|l|+1)}]}$$

is the normalization constant, $z = x + \mathrm{i}y$ is the imaginary displacement from the origin, $L_k^{|l|}(x)$ is a Laguerre polynomial, and $a^2 = \overline{h}/(2\omega m^*)$. The associated eigenenergy is

$$\epsilon_{kl} = \overline{h}\omega[2k + |l| + 1] - \frac{1}{2}l\overline{h}\omega_c. \tag{7}$$

With $\omega_0 = 0$, equation (7) reduces to $\epsilon_{kl} = [k + \frac{1}{2}(|l| - l) + \frac{1}{2}]\overline{h}\omega_c$. Then ϵ_{kl} depends on the quantum number $n = k + (|l| - l)/2$ solely, where n defines the Landau-level index, and l is the quantum number of the angular momentum. For the lowest Landau level, with $n = 0$ (i.e. $k = 0$ and $l \geqslant 0$), the eigenstate of equation (6) can be more succinctly written as

$$|l\rangle = \sqrt{\frac{1}{2^{l+1}\pi l! a^{2(l+1)}}} z^l \exp[-|z|^2/(4a^2)]. \tag{8}$$

This can be qualitatively described as the circular motion of an electron about the origin with angular momentum $l\overline{h}$ and a root mean square orbit radius $\sqrt{(l+1)}a$, since

$$\langle l|r^2|l\rangle = (l + 1)a^2. \tag{9}$$

We now consider the motion of N particles interacting via the unscreened Coulomb potential; the Hamiltonian is

$$H = \sum_{i=1}^{N}\left[\frac{p_i^2}{2m^*} + \frac{1}{2}m^*\omega^2 r_i^2\right] + V(z_1, z_2, \ldots, z_N) - \frac{\omega_c}{2}\hat{L} - g^*\mu_B B\hat{S}_z \tag{10}$$

with

$$V(z_1, z_2, \ldots, z_N) = \sum_{i>j}^{N} \frac{e^2}{4\pi\epsilon_0\epsilon_r|z_i - z_j|} \tag{11}$$

$$\hat{L} = \sum_{i=}^{N}\hat{\ell}_i \qquad \hat{S}_z = \sum_{i=1}^{N}\hat{s}_{zi} \tag{12}$$

where V is the total interaction potential, $\hat{L}$ is the total angular momentum operator, and $\hat{S}_z$ is the Z-component of the total spin.

To solve the eigenequation

$$H\Psi = E\Psi \tag{13}$$

we expand the trial wavefunction in terms of Slater determinants composed of single-particle states:

$$\Psi = \sum_i a_i |i\rangle \tag{14}$$

where i denotes a set of $3N$ quantum numbers $[k_1 l_1 s_{z1}, k_2 l_2 s_{z2}, \ldots, k_N l_N s_{zN}]$ for brevity. We drop the k-indices for a state with all particles in the lowest Landau level. We further drop the spin index s_z for fully polarized states in the following.

When one diagonalizes equation (13), it is worth noticing the following facts:

(a) Since the particle–particle interaction conserves the total angular momentum, Ψ should be a common eigenstate of operators $\{H, \hat{L}, \hat{S}^2, \hat{S}_z\}$.

(b) The particle–particle interaction modifies the relative mode only; it does not affect the centre-of-mass (CM) mode. If we introduce a CM coordinate $z_{\rm cm}$ and $N-1$ Jacobian relative coordinates $\{\eta_1, \eta_2, \ldots, \eta_{N-1}\}$ given by

$$\begin{aligned} z_{\rm cm} &= \frac{1}{N}(z_1 + z_2 + \cdots + z_N) \\ \eta_1 &= \sqrt{\frac{1}{2}}(z_2 - z_1) \\ \eta_2 &= \sqrt{\frac{2}{3}}[z_3 - (z_1 + z_2)/2] \\ &\vdots \\ \eta_j &= \sqrt{\frac{j}{j+1}}[z_{j+1} - (z_1 + z_2 + \cdots + z_j)/j] \\ &\vdots \end{aligned} \tag{15}$$

then the operators H and $\hat{L}$ will split into two independent parts:

$$\begin{aligned} H &= H_{\rm rel} + H_{\rm cm} \\ \hat{L} &= \hat{L}_{\rm rel} + \hat{L}_{\rm cm} \end{aligned} \tag{16}$$

where $\{H_{\rm cm}, \hat{L}_{\rm cm}\}$ describe the CM mode, and $\{H_{\rm rel}, \hat{L}_{\rm rel}\}$ describe the relative mode. The CM motion is equivalent to that of a fictitious particle with particle mass Nm^* and charge Ne. Hence $H_{\rm cm}$ is identical to equation (5), the smallest eigenvalue of which is $E_{\rm cm} = \hbar\omega$ occurring at $L_{\rm cm} = 0$ in the lowest Landau level. We further require that Ψ also be an eigenstate of $H_{\rm cm}$. To guarantee that the lowest state obtained from the numerical diagonalization is the ground state of the CM motion and has the expected total spin, we add an operator $C_1(H_{\rm cm} - \hbar\omega) + C_2(\hat{S}^2 - S(S+1)\hbar^2)$ to H, where C_1 and C_2 are two sufficiently large positive numbers, and S is the expected value of the total spin quantum number.

(c) To obtain quantitatively very accurate spectra, it is necessary to include basis states of several higher Landau levels in the diagonalization, especially in the low-B-field regime. However, we find that the inclusion of higher Landau levels in the basis space does not change the qualitative features (i.e., the magic numbers). Thus it is justified to assume that all electrons are in the lowest Landau level in order to understand the underlying physics well. Within the lowest Landau level, the lowest eigenenergy of a given state (N, L, S) can be written as

$$E(N, L, S) = L(\omega - \omega_c/2) + N\hbar\omega - g^*\mu_B B\hbar S + \langle \Psi^1_{LS} | V(z_1, z_2, \ldots, z_N) | \Psi^1_{LS} \rangle \tag{17}$$

where $S_z = S$ has been assumed, and Ψ^1_{LS} is the lowest eigenstate of a state (N, L, S).

We further introduce a set of hyperspherical coordinates in the following manner:

$$\begin{aligned}
\eta_1 &= \rho\cos(\alpha_1)\mathrm{e}^{\mathrm{i}\varphi_1} \\
\eta_2 &= \rho\sin(\alpha_1)\cos(\alpha_2)\mathrm{e}^{\mathrm{i}\varphi_2} \\
&\vdots \\
\eta_{N-2} &= \rho\sin(\alpha_1)\sin(\alpha_2)\cdots\sin(\alpha_{N-3})\cos(\alpha_{N-2})\mathrm{e}^{\mathrm{i}\varphi_{N-2}} \\
\eta_{N-1} &= \rho\sin(\alpha_1)\sin(\alpha_2)\cdots\sin(\alpha_{N-3})\sin(\alpha_{N-2})\mathrm{e}^{\mathrm{i}\varphi_{N-1}}
\end{aligned} \tag{18}$$

where φ_i is the polar angle of η_i. Physically, the hyper-radius

$$\rho = (|\eta_1|^2 + |\eta_2|^2 + \cdots + |\eta_{N-1}|^2)^{1/2}$$

measures the size; the angular variables $\Omega \equiv \{\alpha_1, \ldots, \alpha_{N-2}; \varphi_1, \ldots, \varphi_{N-1}\}$ measure the shape and the orientation of the system. The wavefunction for N particles all in the lowest Landau level separates into

$$\Psi^k_{LS} = R_L(\rho)Y^k_{LS}(\Omega) \tag{19}$$

where

$$R_L(\rho) = \sqrt{\frac{2}{(2a^2)^{L+N-1}(L+N-2)!}}\rho^L \exp[-\rho^2/(4a^2)]. \tag{20}$$

The total Coulomb interaction energy function can be rewritten as

$$V(z_1, z_2, \ldots, z_N) \equiv \frac{e^2}{4\pi\epsilon_0\epsilon_r}\frac{U(\Omega)}{\rho}. \tag{21}$$

We also observe that

$$\langle R_L|\frac{1}{\rho}|R_L\rangle = \frac{[2(L+N-2)-1]!!}{2^{L+N-2}(L+N-2)!}\sqrt{\frac{\pi}{2a^2}} \tag{22}$$

which decreases monotonically with the increase of L and tends to the limit $1/\sqrt{2(L+N)a^2}$. The average Coulomb energy in the lowest eigenstate can then be expressed as

$$\langle\Psi^1_{LS}|V(z_1, z_2, \ldots, z_N)|\Psi^1_{LS}\rangle = \frac{e^2}{\sqrt{2\pi}\epsilon_0\epsilon_r a}\frac{[2(L+N-2)-1]!!}{2^{L+N}(L+N-2)!}\lambda(N, L, S) \tag{23}$$

where $\lambda(N, L, S)$ is defined by

$$\lambda(N, L, S) = \langle Y^1_{LS}|U(\Omega)|Y^1_{LS}\rangle \tag{24}$$

which is a function of N, L, and S, and is independent of the dynamical parameters m^*, B, and ω_0, etc.

3. Numerical results

Our calculations have been performed for systems containing 3 to 8 electrons. For $N = 3$ and 4, all possible spin configurations have been covered. For $N \geqslant 5$, only the fully polarized states have been considered for brevity. In all cases, the results are for quantum dots created in GaAs (i.e. $m^* = 0.067m_e$, $g^* = 0.044$, $\epsilon_r = 13.1$) with $\omega_0 = 3.6$ meV [8].

In figure 1, the calculated λ is presented as a function of L, separately for different N and S. This quantity is the average interaction energy when the hyper-radius ρ is fixed to unity. Thus it is independent of the size of the system and provides us with information about particle correlation on the $\rho = 1$ hypersphere. Globally speaking, each λ in figure 1 decreases with the increase of L and tends to the classical value of the interaction energy in the equilibrium

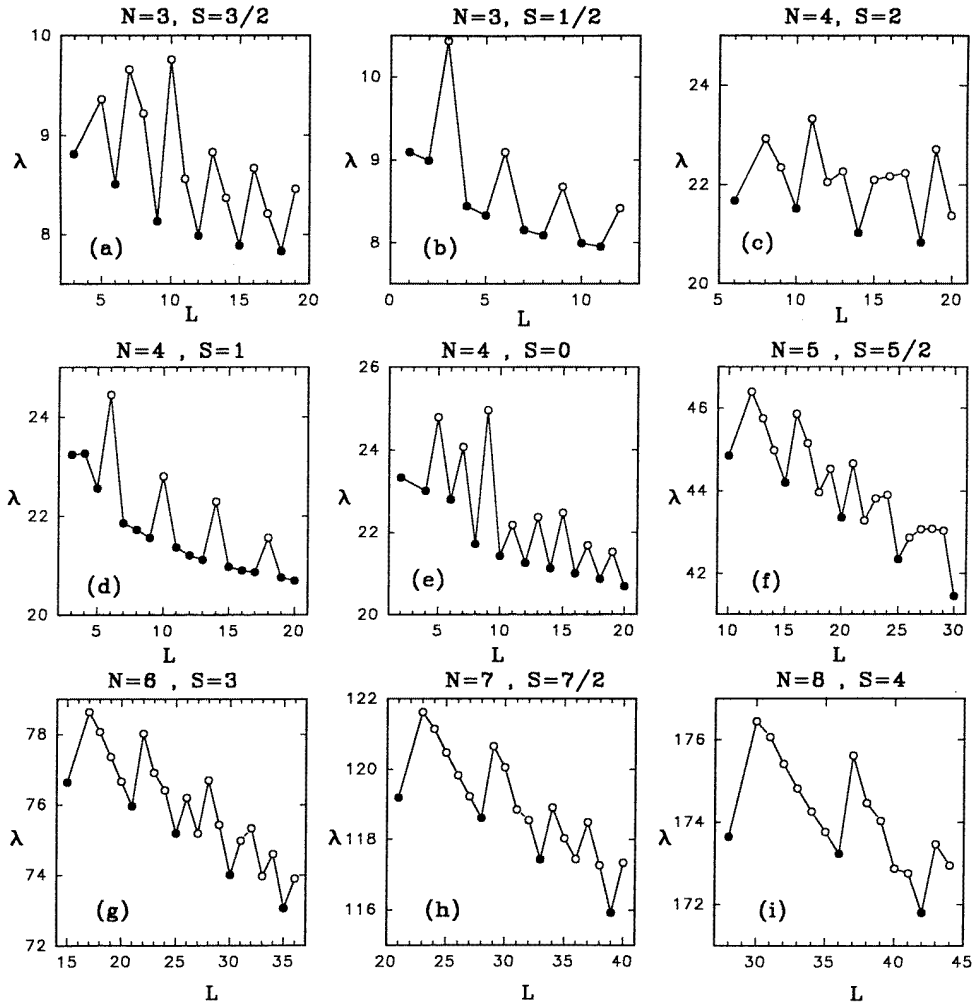

Figure 1. λ, defined in equation (24), is presented as a function of L, separately for different N and S. Only the $S = N/2$ states are presented for $N = 5$ to 8. The black dots denote the states that can become the lowest one in a magnetic field. The hollow dots denote the states that never become the lowest one. There are no states with $L < N(N-1)/2$, and $L = 1 + N(N-1)/2$ at $S = N/2$.

configuration. This is understandable since a quantum system will coincide with its classical counterpart in the limit of large quantum numbers. However, an outstanding feature is that the λ-curves do not vary smoothly but show many downward cusps, implying that at some special (magic) values of L the system has a particularly low interaction energy compared to the cases for other L-values. This results in fluctuation of λ with L. The fluctuation amplitude decreases with the increase of L and is expected to disappear in the classical limit.

To be more precise, for $N = 3, 4, 5$ in the fully polarized states, λ is particularly low when

$$L = Nk + N(N-1)/2 \qquad (k = 0, 1, 2, \ldots). \tag{25}$$

(These values are shown as black dots in figure 1.) For the unpolarized states, the rules are more trivial: particularly low λ occurs at $L \neq 3k$ for $N = 3$ and $S = 1/2$ (see figure 1(b)), at

$L \neq 4k + 2$ for $N = 4$ and $S = 1$ (see figure 1(*d*)), and at $L = 2k$ for $N = 4$ and $S = 0$ (see figure 1(*e*)).

The simple rule of equation (25) is valid for $N = 6, 7, 8$ only with $k = 0, 1$. For larger L, the downward cusps occur at

$$L = (N - 1)k + N(N - 1)/2 \tag{26}$$

for the fully polarized states.

Besides those mentioned above, there are some other minor downward cusps detectable from figure 1 for the polarized states. These are at $L = 12$ for $N = 4$; $L = 13, 22$ for $N = 5$; $L = 27, 33$ for $N = 6$; and $L = 36$ for $N = 7$.

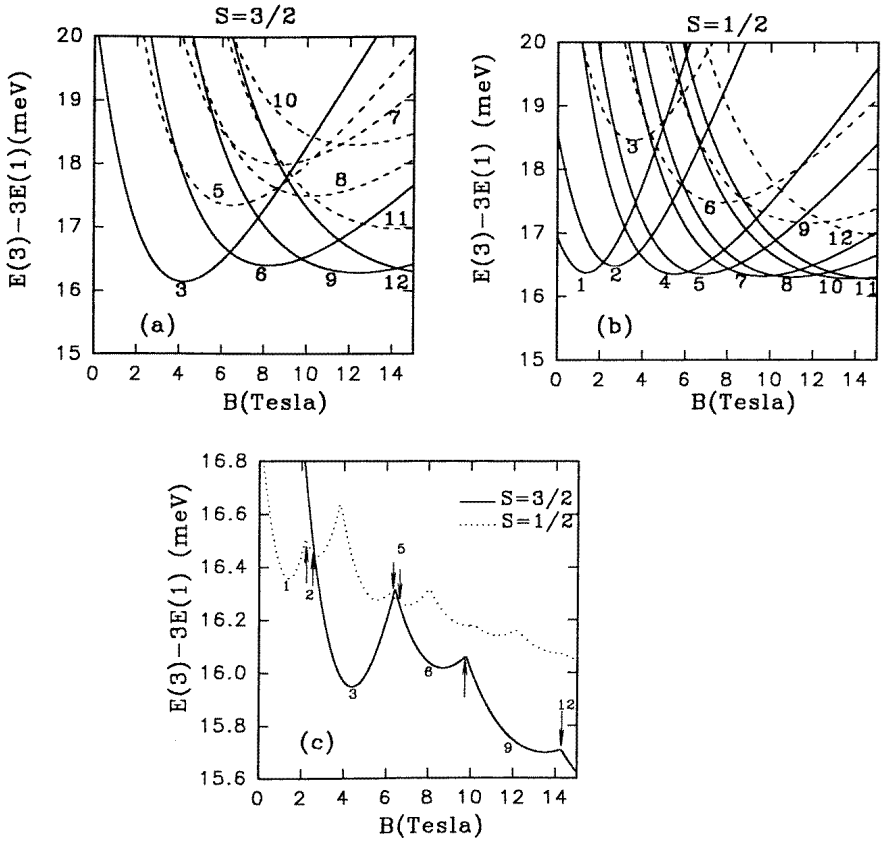

Figure 2. In (*a*) and (*b*), the lowest eigenenergy of a state (L, S) is presented as a function of B for $N = 3$. $E(3)$ is the many-particle eigenenergy defined in equation (17), and $E(1) \equiv \hbar\omega$ is the single-particle energy; the spin term $-g^*\mu_B BS$ is not included. Numbers in the figures indicate the angular momenta L of the states. In (*c*), the lowest energies in different spin configurations are presented together for comparison; here the spin term $-g^*\mu_B BS$ has been included; arrows point to the positions where an L-transition and/or an S-transition take place in the ground state.

Since experimentally a quantum dot is studied by applying a magnetic field in the perpendicular direction, the evolution of eigenenergies in a magnetic field is important to experimentalists. To see where the lowest eigenstate occurs in a magnetic field, we drew each $E(N, L, S)$ (defined in equation (17)) for a given state (N, L, S) as a function of the external magnetic field in figures 2 and 3 for $N = 3$ and 4 respectively; from these figures

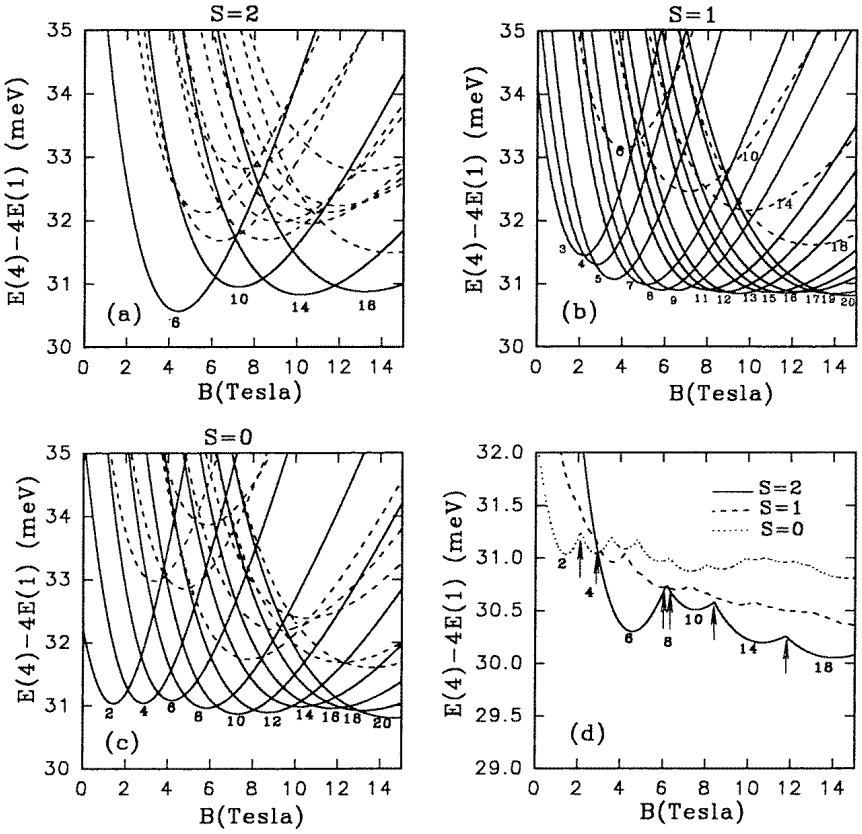

Figure 3. As figure 2, but for $N = 4$.

we see that with the increase of B the lowest state occurs at higher and higher L. Therefore there is an L-transition in quantum dots in a varying magnetic field. This can be qualitatively understood as follows: the orbit radius for the circular motion of an electron in a quantum dot is proportional to l and a (see equation (9)); the latter decreases with the increase of B. Thus electrons will jump to orbits with higher l to avoid the increase of the repulsive interaction energy when the magnetic field strength is increased. We find that if λ is taken to be a constant or a monotonically decreasing function of L, then each state of L can become the lowest and the L-transition takes place continuously; when λ takes the true values as shown in figures 2 and 3, only some of the Ls can become the lowest state and the others never become the lowest state no matter what values are taken by the dynamical parameters. This suggests the existence of certain selection rules governing the L-transition in a magnetic field.

For $N = 3$ in the states with $S = 3/2$ (see figure 2(a)), the lowest state runs over the well-known $L = 3k$ ($k = 1, 2, 3, \ldots$) sequence; in the states with $S = 1/2$ (see figure 2(b)), it is the $L \neq 3k$ sequence that can become the lowest state of that spin configuration. For $N = 4$, the possible lowest states have $L = 4k + 2$ ($k = 1, 2, 3, \ldots$) for $S = 2$ (see figure 3); $L \neq 4k + 2$ for $S = 1$, and $L = 2k$ for $S = 0$. Comparing figures 2 and 3 with figure 1, one immediately recognizes that the lowest state occurs just at those values of L where the corresponding λ-values are particularly low. Hence we are confident that the selection rules originate from the fluctuating structure of λ.

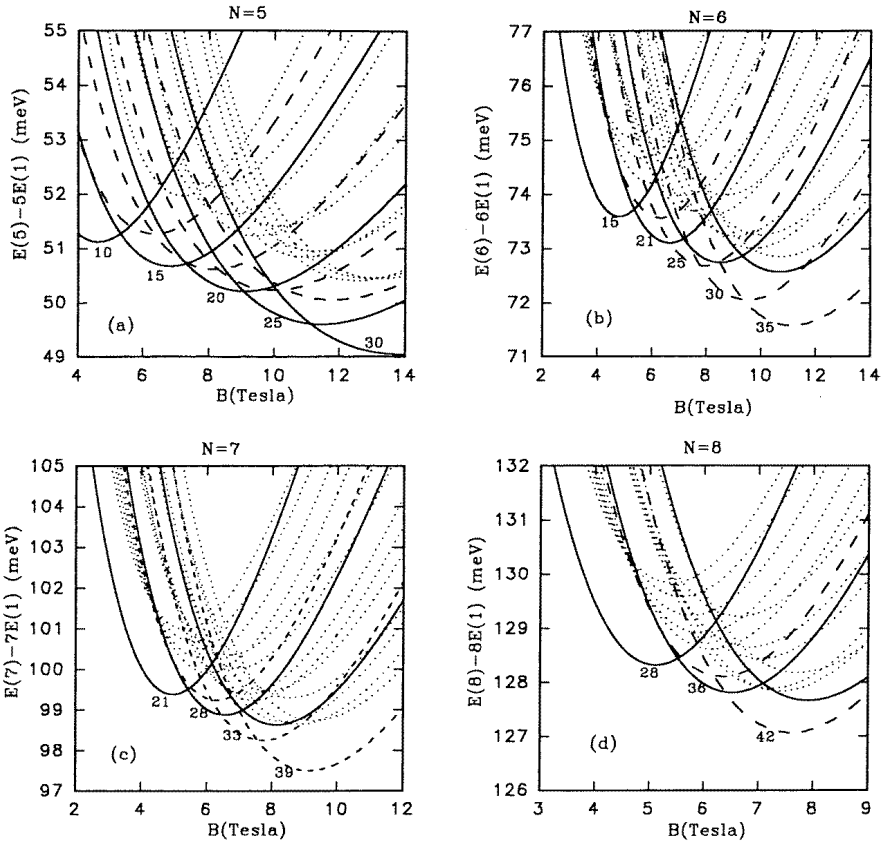

Figure 4. As figure 2, but for $N = 5$ to 8. Only the fully polarized states are presented. The solid curves are for states with $L = Nk + N(N-1)/2$ ($k = 0, 1, 2, \ldots$); the long-dashed curves are for states with $L = (N-1)k + N(N-1)/2$; the dotted curves are for the others.

It should be noted that every possible lowest state detected in figures 2(a), 2(b), 4(a), 4(b), and 4(c) has a chance to become the ground state. To see this clearly, we bring together the lowest eigenenergies of different spin configurations in figures 2(c) and 3(d). Among these curves, the lowest one at a given B is that where the ground state occurs. There is a competition of different spin configurations. The spin term $-g^*\mu_B BS$ in equation (17) makes the polarized state more favourable. As a result, there are complicated spin–spin transitions at low B. The ground state is fully polarized ($S = N/2$) at sufficiently high B-field. For $N = 5$ to 8, the evolution of the eigenenergies in a magnetic field is presented in figure 4. Presumably, we have classified the states into three sequences: sequence L_A for those fulfilling equation (25), sequence L_B for those fulfilling equation (26), and sequence L_C for the others. Generally, a state belonging either to sequence L_A or sequence L_B lies below those belonging to sequence L_C. For $N = 5$ (see figure 4(a)), sequence L_A and sequence L_B are fairly close together, with the former being slightly lower, and the lowest state occurs only in sequence L_A. For $N = 6$ to 8, the lowest state occurs firstly in sequence L_A with $k = 0, 1$ and later in sequence L_B with $k = 2, 3, \ldots$. (Note that the state with $L = N(N-1)/2$ is a crossing of two sequences.) It will soon be clear in the following that states belonging to the same sequence have similar nodal structures.

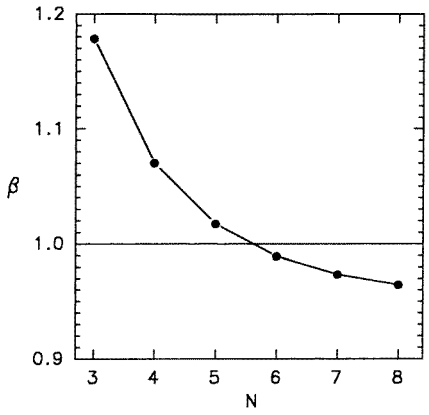

Figure 5. The ratio of the interaction energies in the RP and CRP configurations as a function of N. See equation (27) in the text for the definition of β.

4. Theoretical interpretations

4.1. The geometrical configuration model

In order to reveal the underlying physics of the above numerical data, the task of this section is to show why the interaction energy is low in some states and high in others. We start from some general considerations about an interacting few-particle system. In classical mechanics, a particle can have a definite position, and the interaction energy of a few-particle system can be minimized by forming certain regular equilibrium configurations. For N ($\leqslant 8$) repulsive particles confined in a circular potential, there are two important regular configurations: one is that in which all of the N particles form a regular N-sided polygon (this will be called a regular polygon or RP for short hereafter); another is that in which $N-1$ particles form a regular $(N-1)$-sided polygon and the Nth locates at the centre (this will be called a centred regular polygon or CRP for short). We define the ratio of the interaction energies in these two configurations by

$$\beta = \frac{U(\Omega_{\mathrm{CRP}})}{U(\Omega_{\mathrm{RP}})}. \tag{27}$$

This quantity is presented in figure 5 for $N = 3$ to 8. We notice that $\beta > 1$ for $N \leqslant 5$ and $\beta < 1$ for $N \geqslant 6$. In other words, the RP configuration is more stable than the CRP for $N \leqslant 5$; while for $N \geqslant 6$ the CRP configuration is more stable. The critical point with $\beta = 1$ lies between $N = 5$ and 6. Hence the energies associated with the RP and CRP are close for $N = 5$ and 6. The CRP configuration for $N = 3$ is a dumb-bell with the third particle at the centre (a centred dumb-bell or CDB in short). This configuration corresponds to the saddle point of $U(\Omega)$ in the multicoordinate space and is structurally quite unstable. For other values of N, the RP and CRP configurations are two minima of the corresponding $U(\Omega)$.

In quantum mechanics, a system does not have a rigid geometrical configuration. Instead, we have a probability distribution given by the wavefunction, and the kinetic energy is determined by the curvature of the wavefunction. To have a rigid geometrical configuration is to have a wavefunction of Dirac's delta, which may be very favourable for minimizing the interaction energy but gives infinite kinetic energy of the state. In the lowest eigenenergy state, there is a balance of the two, such that the total energy is minimized. Thus it is natural to suppose that the lowest state should have its wavefunction smoothly (without nodes) distributed

in the vicinity of and peaking at the equilibrium point. Besides the dynamics, the permutation symmetry plays an important role in identical-particle systems. For non-interacting particle systems, the symmetry constraints are prescribed by how the particles can fill the single-particle states. In strongly interacting systems, the concept of single-particle states is no longer valid. We must consider the symmetry constraints globally. As we will see in the following, the equilibrium configuration may in some cases be prohibited by symmetries; this does not have a classical counterpart.

Let us decompose the N-body wavefunction according to the spin couplings in the following manner:

$$\Psi_{LS} = \sum_{\nu_1 \cdots \nu_{N-2}} \Phi_{[L;\nu_1 \cdots \nu_{N-2}S]}(z_1, z_2, \ldots, z_N)|(s_1 s_2)_{\nu_1}(\nu_1 s_3)_{\nu_2} \cdots (\nu_{N-2} s_N)_S\rangle \tag{28}$$

where $\Phi_{[L;\nu_1 \cdots \nu_{N-2}S]}$ is the spatial part; $|(s_1 s_2)_{\nu_1}(\nu_1 s_3)_{\nu_2} \cdots (\nu_{N-2} s_N)_S\rangle$ is the spin part: s_1 and s_2 are coupled to ν_1 and ν_1, and s_3 is coupled to ν_2, etc. If the particles form a RP, a rotation of $2\pi/N$ about the origin, which produces a phase factor of $\exp(\mathrm{i}\, 2\pi L/N)$ when operating on the wavefunction, is equivalent to a cyclic permutation of the N particles. This leads to the following equation:

$$\exp[\mathrm{i}\, 2\pi L/N]\Phi_{[L;\nu_1 \cdots \nu_{N-2}S]}(z_1^0, z_2^0, \ldots, z_N^0) = \Phi_{[L;\nu_1 \cdots \nu_{N-2}S]}(z_N^0, z_1^0, z_2^0, \ldots, z_{N-1}^0) \tag{29}$$

where we have assumed that the particles form a RP and set $z_j^0 = z_1^0 \exp[\mathrm{i}\, 2\pi(j-1)/N]$ without any loss of generality. $\Phi_{[L;\nu_1 \cdots \nu_{N-2}S]}(z_N^0, z_1^0, z_2^0, \ldots, z_{N-1}^0)$ can be re-expanded in the following manner:

$$\Phi_{[L;\nu_1 \cdots \nu_{N-2}S]}(z_N, z_1, z_2, \ldots, z_{N-1}) = \sum_{\nu_1' \cdots \nu_{N-2}'} A^{[\nu_1 \cdots \nu_{N-2}S]}_{[\nu_1' \cdots \nu_{N-2}'S]} \Phi_{[L;\nu_1' \cdots \nu_{N-2}'S]}(z_1, z_2, \ldots, z_N) \tag{30}$$

where the expansion coefficients can be obtained analytically with the aid of representation theory for symmetric group S_N and eventually be expressed in terms of the Clebsch–Gordan coefficients [29]. Combining equations (29) and (30), we obtain a set of homogeneous linear equations for $\{\Phi_{[L;\nu_1 \cdots \nu_{N-2}S]}(z_N^0, z_1^0, z_2^0, \ldots, z_{N-1}^0)\}$. Non-vanishing solutions exist only when

$$\det\{A^{[\nu_1 \cdots \nu_{N-2}S]}_{[\nu_1' \cdots \nu_{N-2}'S]} - \exp[\mathrm{i}\, 2\pi L/N]\delta_{[\nu_1 \cdots \nu_{N-2}],[\nu_1' \cdots \nu_{N-2}']}\} = 0 \tag{31}$$

where $\delta_{[\nu_1 \cdots \nu_{N-2}],[\nu_1' \cdots \nu_{N-2}']} = \delta_{\nu_1,\nu_1'}\delta_{\nu_2,\nu_2'} \cdots \delta_{\nu_{N-2},\nu_{N-2}'}$. Similar equations can be constructed for $\{\Phi_{[L;\nu_1 \cdots \nu_{N-2}S]}\}$ in the CRP configuration.

Consider the simplest case of fully polarized states ($S = N/2$); there is only one component of the wavefunction ($\nu_i = (i+1)/2$, $i = 1, \ldots, N-2$), and

$$A^{[\nu_1 \cdots \nu_{N-2}S]}_{[\nu_1 \cdots \nu_{N-2}S]} = (-1)^{N-1}. \tag{32}$$

Let $\Psi_L(\mathrm{RP})$ be the value of the spatial wavefunction at the RP configuration in the fully polarized state. From equations (28)–(32) we observe that $\Psi_L(\mathrm{RP}) \neq 0$ only when $L = Nk + N(N-1)/2$ (k being an integer). When $\Psi_L(\mathrm{RP}) \neq 0$, it is called an RP-accessible state. When $\Psi_L(\mathrm{RP}) = 0$, the RP configuration is a node of the wavefunction and it is called an RP-inaccessible state. Similarly, we have $\Psi_L(\mathrm{CRP}) \neq 0$ only when $L = (N-1)k + N(N-1)/2$ for the polarized states. Hence it is now clear that sequence L_A is just composed of states for which the RP configuration is accessible by symmetries; sequence L_B are states for which the CRP configuration is accessible; and sequence L_C are states for which the RP and CRP configurations are both prohibited by symmetries.

For the unpolarized states ($S < N/2$), there is more than one component of the wavefunction. As an example, we consider the simplest case of $N = 3$ for the states with

$S = 1/2$. The equilibrium configuration for $N = 3$ is an equilateral triangle (denoted by ET); we have

$$\begin{pmatrix} A^{[1\frac{1}{2}]}_{[1\frac{1}{2}]} & A^{[1\frac{1}{2}]}_{[0\frac{1}{2}]} \\ A^{[0\frac{1}{2}]}_{[1\frac{1}{2}]} & A^{[0\frac{1}{2}]}_{[0\frac{1}{2}]} \end{pmatrix} = \begin{pmatrix} -\frac{1}{2} & \frac{\sqrt{3}}{2} \\ -\frac{\sqrt{3}}{2} & -\frac{1}{2} \end{pmatrix}. \tag{33}$$

Combining equation (31) and equation (33), we obtain that non-vanishing $\Phi_{[L,1,\frac{1}{2}]}(\mathrm{ET})$ and $\Phi_{[L,0,\frac{1}{2}]}(\mathrm{ET})$ occur only when $L \neq 3k$.

For $N = 4$, the equilibrium configuration is a square (denoted by SQ). Using similar arguments, we find that the SQ configuration is not prohibited by symmetries only when $L \neq 4k + 2$ for $S = 1$ and $L = 2k$ for $S = 0$.

On comparing what was obtained here and the numerical results given in figures 1–4, it is now clear that the lowest possible states are just those for which the equilibrium configuration is accessible by symmetries, i.e. the lowest states possible for $N \leqslant 5$ are those for which the RP configuration is accessible; for $N = 6, 7, 8$ they are the RP- and/or CRP-accessible states.

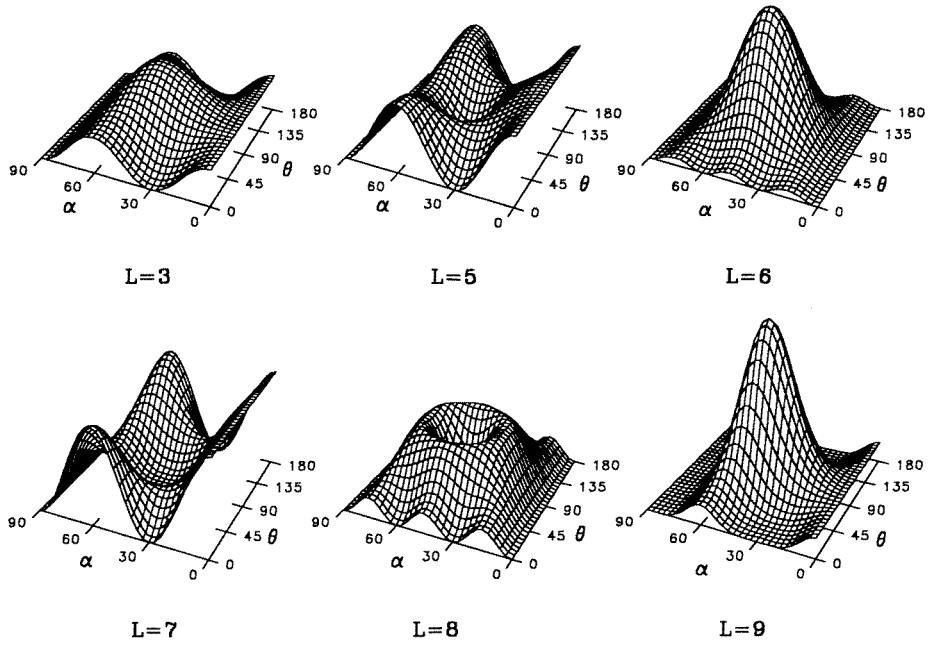

Figure 6. $|Y^1_{LS}|^2$ as a function of (α, θ) for $N = 3$ and $S = 3/2$.

To see clearly what happens to the wavefunction when the equilibrium configuration is accessible or prohibited by symmetries, as an example we present in figure 6 the angular part of the wavefunction for $N = 3$ in the state $S = 3/2$ as a function of (α, θ), which provides us with all of the information about particle correlations. α and θ are then defined by

$$\tan\alpha = \frac{|\eta_1|}{|\eta_2|} \tag{34}$$

$$\theta = \varphi_2 - \varphi_1 \tag{35}$$

(see equation (18) and figure 7). In the (α, θ) plane, the points $(30^\circ, 0)$, $(30^\circ, 180^\circ)$ and the line $\alpha = 90^\circ$ correspond to $z_{23} = 0$, $z_{13} = 0$, and $z_{12} = 0$ respectively; they are nodes

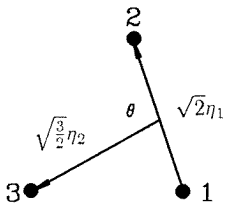

Figure 7. Jacobi coordinates for a three-body system.

of any antisymmetric states; points $(60^\circ, 0)$, $(60^\circ, 180^\circ)$ and the line $\alpha = 0$ (i.e. $\eta_2 = 0$) correspond to the CDB, which is a node of $L =$ even states, since in a dumb-bell a rotation of 180° is equivalent to an exchange of the two particles at the ends; the central point $(45^\circ, 90^\circ)$ corresponds to the equilibrium configuration (an ET). In an ET-accessible state ($L = 3k$), the distribution of the wavefunction is simply a tower located at $(45^\circ, 90^\circ)$, implying that the ET is the dominant configuration such that the average interaction energy is particularly low. $(45^\circ, 90^\circ)$ is a node of the wavefunction in all ET-inaccessible states. As a result, the wavefunction can only distribute away from $(45^\circ, 90^\circ)$ such that it looks like a volcano and the system does not have a dominant configuration. The interaction energy is not minimized in this state. The other N-particle wavefunctions show similar structures [25, 26].

Since there are two equilibrium configurations for $N \geqslant 4$, there are two sequences of magic numbers, i.e., sequence L_A and sequence L_B in the fully polarized states (note that the CRP is accessible for all $S < N/2$ states). For $N = 4$, the RP configuration is much more stable than the CRP, and sequence L_B appears only as minor downward cusps (e.g., see $L = 12$ in figure 1(c)). Occasionally an $L \in$ sequence L_B is adjacent to an $L' \in$ sequence L_A and the minor downward cusp is not seen (see $L = 9, 15$ in figure 1(c)). The existence of two sequences of magic numbers is more evident with $N = 5$ and 6, since the CRP configuration is then more competitive with the RP in energy.

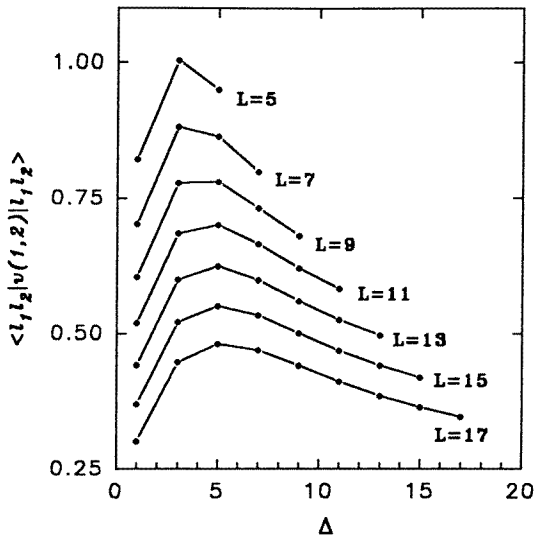

Figure 8. The average two-particle interaction energy as a function of $\Delta = |l_2 - l_1|$ for some given L.

4.2. The ℓ-configuration model

In this subsection, we provide an alternative interpretation for the fully polarized states. We start by considering the cyclic motion of two electrons in a non-perturbative antisymmetric state of $|l_1 l_2\rangle$. To see how the electrons can minimize their interaction energy, in figure 8 we present the average interaction energy as a function of Δ ($\equiv|l_2 - l_1|$) for some fixed L ($\equiv l_1 + l_2$). For a prescribed L, there are two effective ways for the particles to reduce their interaction energy. The first is to fill the orbits compactly (i.e. to have $\Delta = 1$) so that they move at the smallest relative velocity and meet each other least frequently. In the classical limit (i.e., $l \gg 1$), this describes a state of two electrons rotating at the same speed and with a phase difference of π, since

$$|l, l+1\rangle \sim z_1^l z_2^l (z_1 - z_2) \exp[-(|z_1|^2 + |z_2|^2)/(4a^2)] \tag{36}$$

whose maximum amplitude occurs when $z_1 = -z_2$. The second is to have $\Delta = L$ (i.e., $l_1 = 0$, $l_2 = L$) so that they can keep their orbits as far apart as possible. $|0, L\rangle$ describes a state of two electrons with one undergoing a zero-point oscillation about the origin and the second rotating around it. As can be seen in figure 8, the first way is more effective than the second. Hence it is reasonable to expect the compact-filling configuration to be pursued by other small N-particle systems. However, in a compact cluster, the number of particle pairs that are not adjacent ($=(N-1)(N-2)/2$) and their differences in angular momentum increase rapidly. This gradually makes the compact filling unfavourable with increase of N. Hence for a large N a configuration with the particles divided into two or more well separated compact sub-clusters may be superior to one single compact cluster.

After numerically diagonalizing the Hamiltonian, we carefully analysed the wavefunctions and found that each state of sequence L_A is dominated by a Slater determinant of $|l, l+1, \ldots, l+N-1\rangle$ (which will be called a compact state hereafter [30]) with some mixings of other Slater determinants having the same L; for $N \geqslant 4$, each state of sequence L_B is dominated by a Slater determinant of $|0, l+1, l+2, \ldots, l+N-1\rangle$ (which will be called a quasi-compact state hereafter). In figure 9, we gave some examples to show this. Note that a single Slater determinant is scarcely an eigenstate of $H_{\rm cm}$; mixing of basis states is inevitable. A noteworthy feature in figure 9 is that the eigenstate becomes more dominated by a single Slater basis state with increase of N. Bearing in mind that the CM correlation is a strong constraint on the motion of small-N particles but a weak one on that of large-N particles [31], the feature strongly suggests that the mixings are mainly caused by the CM correlation. We justified this supposition by constructing a trial wavefunction in the following manner:

$$\Psi_{\rm trial} = \hat{P}|l, l+1, \ldots, l+N-1\rangle \tag{37}$$

for $L = Nl + N(N-1)/2$, or

$$\Psi_{\rm trial} = \hat{P}|0, l+1, \ldots, l+N-1\rangle \tag{38}$$

for $L = (N-1)l + N(N-1)/2$, where $\hat{P}$ is an operator projecting the state onto the ground state of $H_{\rm cm}$. In table 1 we have listed the overlap of $\Psi_{\rm trial}$ with the true state Ψ obtained numerically for $N = 3$. There is a good agreement between $\Psi_{\rm trial}$ and Ψ. The agreement is approximately at the same level for other values of N. Thus we can qualitatively say that the mixings mainly result from the CM correlation, and that the effect of particle interaction is to select, among all possible ℓ-configurations, the most favourable one such that the interaction energy is minimized.

In the ℓ-configuration space, we have a particularly simple picture for the ground-state transitions of quantum dots in an increasing magnetic field in the infinite-Zeeman-energy limit ($g^* \to \infty$). For $N \leqslant 5$, the compact filling is the most stable and each possible ground

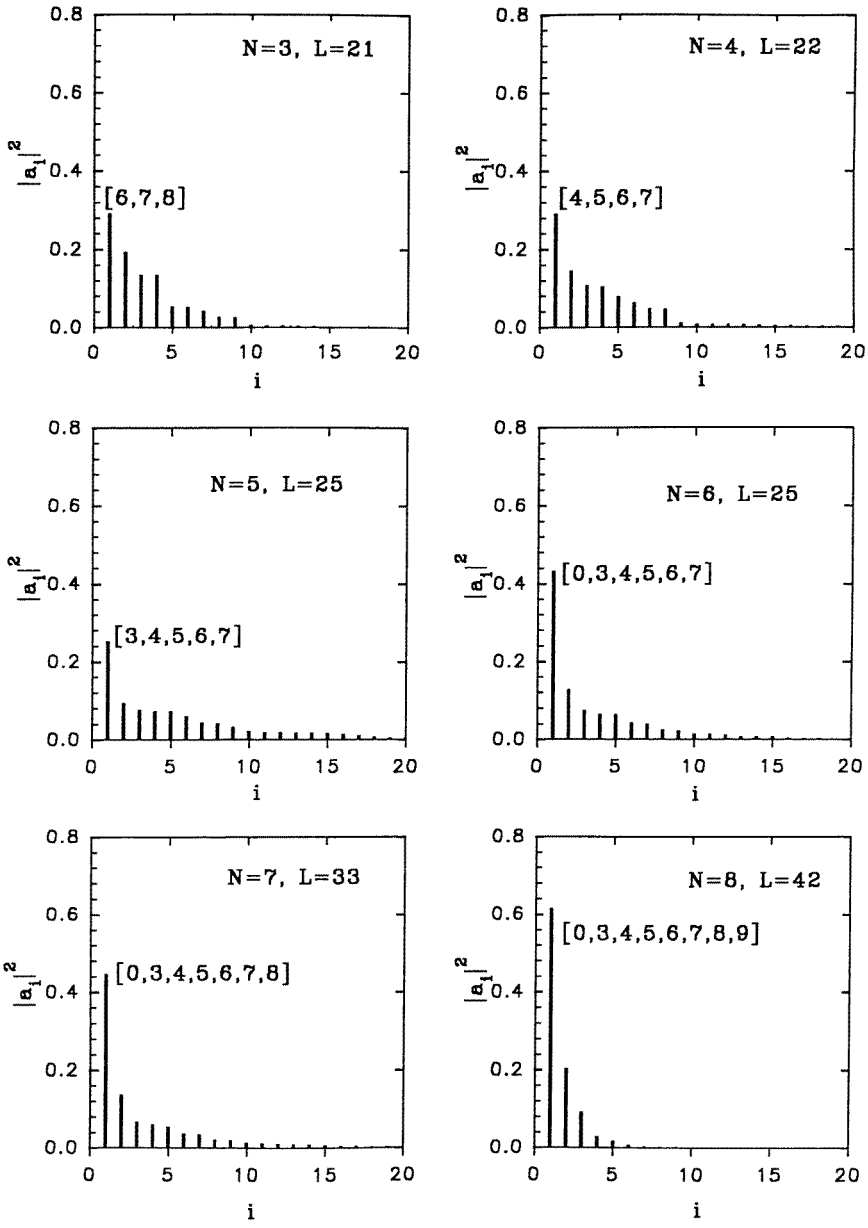

Figure 9. Mixing of basis states in the lowest eigenenergy states. a_i is defined in equation (14) in the text. Bases are numbered in decreasing order of $|a_i|^2$. The bracket indicates the ℓ-configuration of the dominant basis state.

state is dominated by a compact basis state. The ground-state transition obeys a selection rule $\Delta L = N$ (see figure 10(a) for $N = 3$). For $N = 6, 7, 8$, the compact filling is no longer the most stable. However, when L is small (i.e., $L < 2(N-1)+N(N-1)/2$), there is not enough room for the particles to divide into two well separated clusters; the first two possible ground states are compact states with $L = N(N-1)/2$ and $N + N(N-1)/2$ respectively. With

Table 1. Overlaps of the trial three-body wavefunction Ψ_{trial} from equation (37) with Ψ, calculated in the following manner: $\langle\Psi_{\text{trial}}|\Psi\rangle/(\langle\Psi_{\text{trial}}|\Psi_{\text{trial}}\rangle\langle\Psi|\Psi\rangle)^{1/2}$. Ψ is the lowest-energy eigenstate of angular momentum $L \equiv l_1 + l_2 + l_3 = 3k$ with $S = 3/2$, obtained numerically with an inter-electronic potential of $1/r$.

L	$[l_1, l_2, l_3]$	Overlaps
3	[0, 1, 2]	1
6	[1, 2, 3]	1
9	[2, 3, 4]	0.990 9971
12	[3, 4, 5]	0.971 5041
15	[4, 5, 6]	0.971 5773
18	[5, 6, 7]	0.974 3785
21	[6, 7, 8]	0.976 4479
24	[7, 8, 9]	0.978 4010

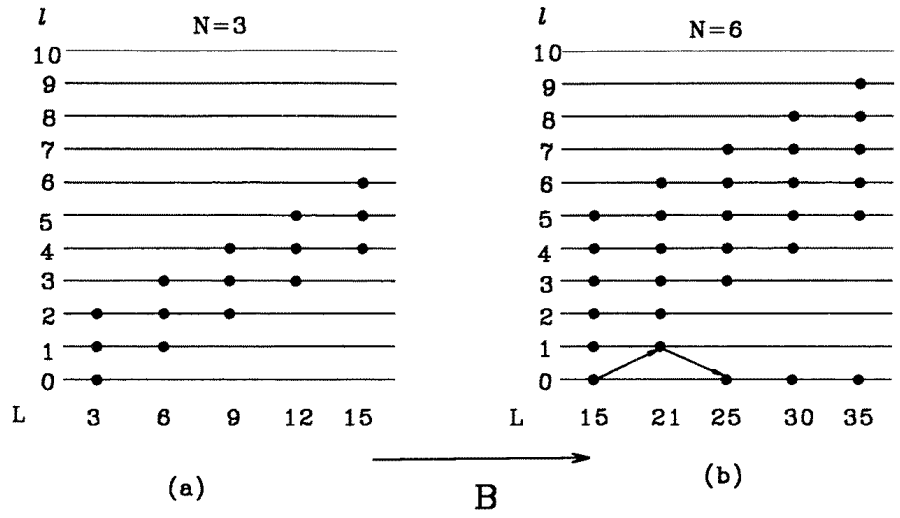

Figure 10. Intuitive pictures for the ground-state transition in the space of single-particle angular momentum for $N = 3$ and 6.

larger L, more single-particle orbits are open; the N-particle compact cluster splits up into an $(N-1)$-particle compact cluster and a single particle in the $l = 0$ orbit (see figure 10(b) for $N = 6$). Possible ground states then have angular momenta of $L = (N-1)k + N(N-1)/2$ ($k = 2, 3, 4, \ldots$). It is quite tempting to investigate whether further splittings happen for larger (N, L). Unfortunately this is beyond the scope of our numerical computation.

4.3. The relationship of the two models

In this subsection, we discuss the relationship of the geometrical configuration model and the ℓ-configuration model by justifying two suppositions: (a) that for N particles to compactly fill the orbits is geometrically to form a RP; (b) that for $N-1$ particles to compactly fill the orbits and the Nth to fill the $l = 0$ orbit is geometrically to form a CRP.

First of all, we notice that a RP-accessible state (i.e., a state in sequence L_A) is just one for which N particles can fill the orbits compactly, and a CRP-accessible state (i.e., a state in sequence L_B) is just one for which $N-1$ particles can fill the $l > 0$ orbits compactly, leaving

the $l = 0$ orbit for the Nth particle.

To show that the dominant geometrical configuration of a compact state is a RP, we write the wavefunction explicitly as

$$|l, l+1, \ldots, l+N-1\rangle \sim z_1^l z_2^l \cdots z_N^l \prod_{i>j}^{N} (z_i - z_j) \exp[-(|z_1|^2 + |z_2|^2 + \cdots + |z_N|^2)/(4a^2)]. \tag{39}$$

This describes the cyclic motion of N particles in a circular band of inner radius $\sqrt{(l+1)}a$ and outer radius $\sqrt{(l+N)}a$. The Pauli exclusion effectively separates the particles from each other inside the band. Hence, with $l \gg N$, equation (39) qualitatively describes the circular motion of N particles with the same radii and a phase difference of $2\pi/N$ for any pair of adjacent particles (i.e., a rotating RP). Similarly, with $l \gg N$, $|0, l, l+1, \ldots, l+N-2\rangle$ describes a rotating CRP. The effect of CM correlation further enhances the formation of a RP or a CRP.

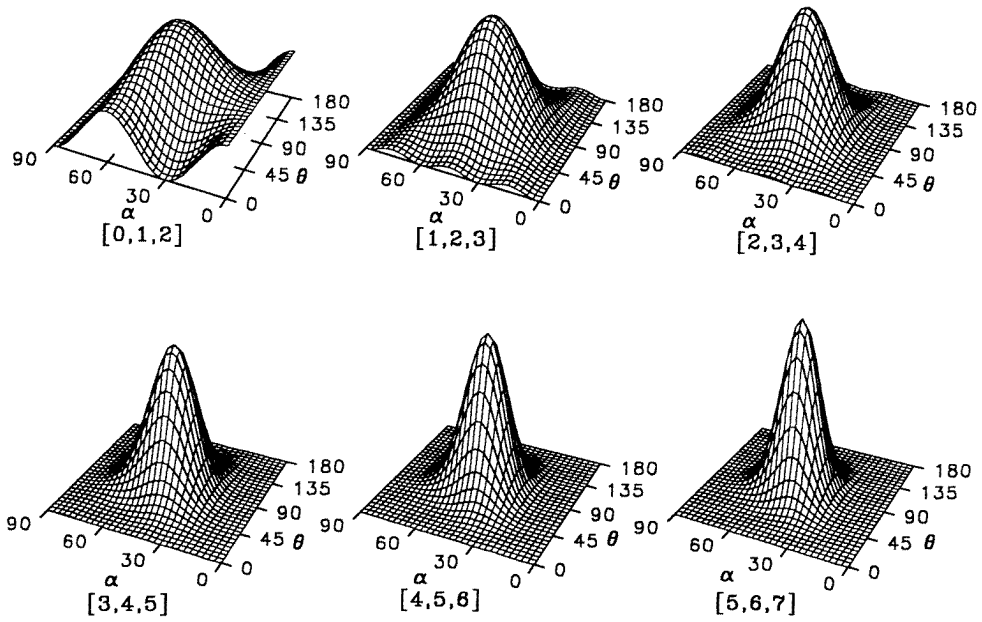

Figure 11. $|Y_{\text{trial}}|^2$, the hyper-angular part of $|\Psi_{\text{trial}}|^2$, as a function of (α, θ) for $N = 3$ in the compact states.

The introduction of hyperspherical coordinates separates each of equations (37)–(39) into the product of a radial part and an angular part as before. As an example, in figure 11, we present the hyper-angular part of $|\Psi_{\text{trial}}|^2$ obtained from equation (37) for $N = 3$, where even for the state $|0, 1, 2\rangle$ (i.e., for $l = 0$ in equation (37)) the dominant role of the ET configuration (the RP configuration for $N = 3$) is evident. In figure 12, the hyper-angular part of $|\Psi_{\text{trial}}|^2$ defined in equation (38) is presented, where the dominant configuration is a CDB (the CRP configuration for $N = 3$). The geometrical configuration becomes better defined (i.e. the wavefunction has sharper peaks) as L increases.

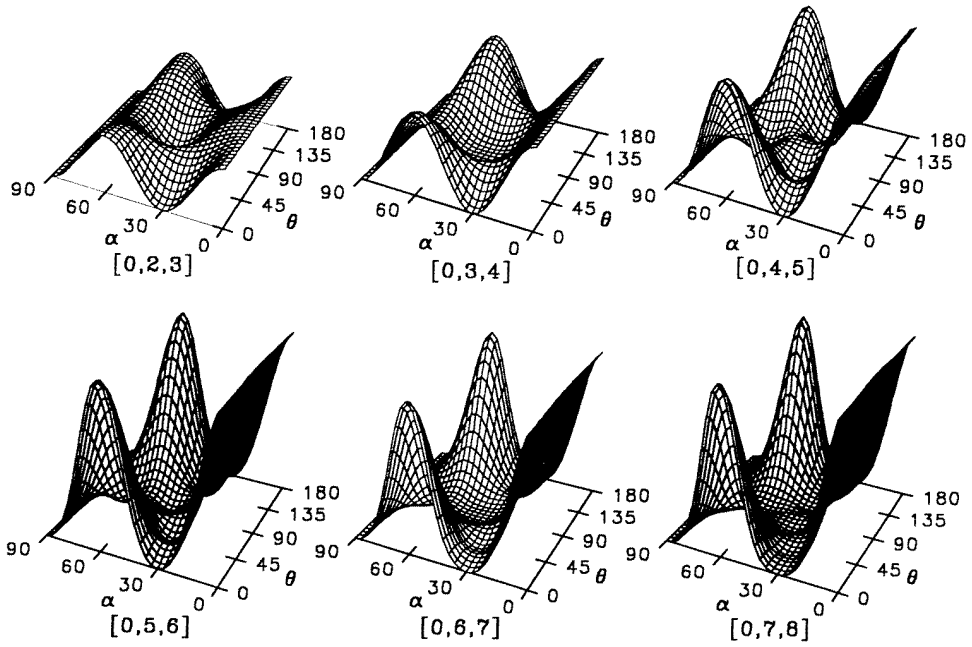

Figure 12. As figure 11, but for the quasi-compact states.

5. Summary

To summarize, in this paper we have presented extensive numerical results for the quantum spectra and particle correlations of systems of few interacting electrons in a parabolic quantum dot and a strong magnetic field. Only the low-lying states have been considered. With all particles in the lowest Landau level, the introduction of hyperspherical coordinates allows the separation of the interaction energy into the product of a radial part and an angular part; the former decreases monotonically with increase of angular momentum, while the latter brings out rich structures. There exist magic angular momenta which give particularly low interaction energy. For $N \geqslant 4$ in the fully polarized states, two sequences of magic angular momenta have been discovered. For the unpolarized states the rules that determine the magic angular momenta are more trivial and strongly depend on (N, S). For the appearance of magic angular momenta, two theoretical models have been proposed.

In the geometrical model, the basic assumption is that the wavefunction should focus on some symmetric configurations. This is a general feature of few-particle systems (but may not apply for a large N). There are two equilibrium configurations for $N \geqslant 4$ (i.e., the RP and CRP). Particularly low interaction energy is obtained when one of them is accessible by symmetries, resulting in two sequences of magic angular momenta for the fully polarized states. For $N \leqslant 5$, sequence L_A is superior to sequence L_B since the RP is more stable than the CRP; for $N > 5$, the CRP is more stable than the RP and sequence L_B becomes dominant.

In the ℓ-configuration model, we provide an independent-particle picture for the motion of interacting particles in the lowest Landau level. There are two important configurations in the ℓ-space, i.e. the compact filling and the quasi-compact filling, which effectively reduce the interaction energy of a few-particle system. Hence particularly low interaction energy is obtained when the compact or quasi-compact filling is accessible. The compact filling is more

effective when $N \leqslant 5$; the quasi-compact filling is superior to the compact filling for $N \geqslant 6$ and sufficiently large L.

Seemingly, the two models are quite different. However, as we have pointed out, they are equivalent to some extent. There is a similarity to the case of some light even–even nuclei (e.g., ^{12}C) for which the α-cluster model and the shell model are both very successful in describing the ground state and some low-lying excited states in nuclear physics [32]. Here the Pauli correlation plays an important role. It blurs the distinction of the two models. The ℓ-configuration model seems to work better than the geometrical one at small L for $N = 6, 7, 8$ where the wavefunction does not have sharp peaks. The geometrical configuration model is on a sounder footing when L is large or the interaction energy is dominant (e.g., in the Wigner-crystal regime), since then the wavefunction has a sharper peak (or peaks). As for systems where the interaction energy is dominant, the true state is a mixture of basis states of many Landau levels, and the ℓ-configuration model developed in this paper on the basis of the lowest Landau level is no longer valid.

Acknowledgments

This work was supported by the Research Committee, City University of Hong Kong, under grant No 7000415, and also in part by the National Natural Science Foundation, grant No 19875018, Guangdong Provincial Natural Science Foundation and Guangzhou Civic Natural Science Foundation, People's Republic of China.

References

[1] Ashoori R C, Stormer H L, Weiner J S, Pfeiffer L N, Pearton S J, Baldwin K W and West K W 1992 *Phys. Rev. Lett.* **68** 3088
[2] Sikorski Ch and Merkt U 1989 *Phys. Rev. Lett.* **62** 2164
[3] Meurer B, Heitman D and Ploog K 1992 *Phys. Rev. Lett.* **68** 1371
[4] Su Bo, Goldman V J and Cunningham J E 1992 *Science* **255** 313
[5] Ashoori R C, Stormer H L, Weiner J S, Pfeiffer L N, Baldwin K W and West K W 1993 *Phys. Rev. Lett.* **71** 613
[6] McEuen P L, Foxman E B, Meirav U, Kastner M A, Meir Y and Wingreen N S 1991 *Phys. Rev. Lett.* **66** 1926
[7] Reed M A, Randall J N, Aggarwal R J, Matyi R J, Moore T M and Wetsel A E 1988 *Phys. Rev. Lett.* **60** 535
[8] Hawrylak P 1993 *Phys. Rev. Lett.* **71** 3347
[9] Kastner M A 1992 *Rev. Mod. Phys.* **64** 849
[10] Laughlin R B 1983 *Phys. Rev.* B **27** 3383
[11] Girvin S M and Jach T 1984 *Phys. Rev.* B **29** 5617
[12] Lai W, Yu K, Su Z and Yu L 1984 *Solid State Commun.* **52** 339
[13] Maksym P A and Chakraborty T 1990 *Phys. Rev. Lett.* **65** 108
[14] Yang S R E, MacDonald A H and Johnson M D 1993 *Phys. Rev. Lett.* **71** 3194
[15] Schmidt T, Tewordt M, Blick R H, Haug R J, Pfannkuche D and von Klitzing K 1995 *Phys. Rev.* B **51** 5570
[16] Maksym P A and Chakraborty T 1992 *Phys. Rev.* B **45** 1947
[17] Hawrylak P and Pfannkuche D 1993 *Phys. Rev. Lett.* **70** 485
[18] Weinmann D, Hausler W and Kramer B 1995 *Phys. Rev. Lett.* **74** 984
[19] Palacios J J, Martin-Moreno L, Chiappe G, Louis E and Tejedor C 1994 *Phys. Rev.* B **50** 5760
[20] Jain J K and Kawamura T 1995 *Europhys. Lett.* **29** 321
[21] Kamilla R K and Jain J K 1995 *Phys. Rev.* B **52** 2798
[22] Seki T, Kuramoto Y and Nishino T 1996 *J. Phys. Soc. Japan* **65** 3945
[23] Dharma-wardana M W C 1995 *J. Phys.: Condens. Matter* **7** 4095
[24] Kawamura T and Jain J K 1996 *J. Phys.: Condens. Matter* **8** 2095
[25] Maksym P A 1993 *Physica* B **184** 385
[26] Maksym P A 1996 *Phys. Rev.* B **53** 10 871
[27] Ruan W Y, Liu Y Y, Bao C G and Zhang Z Q 1995 *Phys. Rev.* B **51** 7942
[28] Bao C G, Ruan W Y and Liu Y Y 1996 *Phys. Rev.* B **53** 10 820

[29] Wigner E P 1959 *Group Theory and its Applications to the Quantum Mechanics of Atomic Spectra* (New York: Academic)
Wigner E P 1955 *Shell Structures* (New York: Wiley)
[30] Note that our definition of compact states is different from Jain's in [20], where the particles are allowed to occupy the higher Landau levels.
[31] In the classical picture, the CM correlation requires that the particles cooperate during their cyclic motion such that the centre of mass is always at the origin.
[32] Wildermuth K and Tang Y C 1977 *A Unified Theory of the Nucleus* (New York: Academic)